

data, suggesting the use of higher order statistics for modeling the radar data.

It is thus evident, that based on the statistical properties of the radar data for a realistic radar target as well as the 2-D images generated, using frequency and aspect data, regions exist that exhibit strong higher order statistics.

III. CONCLUSION

The backscattered field of an Airbus A310 model was measured in a compact range, and frequency data were used to investigate the statistical properties and dominant statistical dependency of measured radar data as a function of aspect angle. The results indicate that the use of higher order statistics or second-order statistics in radar imaging algorithms must be done with care. Second-order statistics may be used most of the time, but the reader must be aware that in certain angle regions higher order statistics must be considered. Although, higher order statistics has many advantages, it is not advisable to use only higher order statistics if most of the measured radar data indicate second-order statistics. If multiple reflections and higher order interactions occur over a specific aspect region, higher order statistics is preferred over second-order statistics to analyze and model the measured radar data. Second-order statistics is likely to be preferred if the radar target is less complex and produces minor multiple reflection and higher order interactions. *A priori* knowledge of the scattering mechanisms contributing to the backscattered field in a certain region is thus required to know the statistics to use in generating radar images.

REFERENCES

- [1] D. L. Mensa, *High Resolution Radar Cross-Section Imaging*. Norwood, MA: Artech House, 1991.
- [2] J. W. Odendaal, E. Barnard, and C. W. I. Pistorius, "Two-dimensional super-resolution radar imaging using the MUSIC algorithm," *IEEE Trans. Antennas Propagat.*, vol. 42, no. 10, pp. 1386–1391, Oct. 1994.
- [3] I. J. Gupta, "High-resolution radar imaging using 2-D linear prediction," *IEEE Trans. Antennas Propagat.*, vol. AP-42, pp. 31–37, Jan. 1994.
- [4] C. L. Nikias and A. P. Petropula, *Higher-Order Spectra Analysis: A Non-Linear Signal Processing Framework*. Englewood Cliffs, NJ: Prentice Hall, 1993.
- [5] E. K. Walton and I. Jouny, "Bispectrum of radar signatures and application to target classification," *Radio Sci.*, vol. 25, pp. 101–113, Mar. 1990.
- [6] P. Niemand and J. W. Odendaal, "Radar imaging using higher order statistics," *Microwave Opt. Technol. Lett.*, vol. 16, no. 1, pp. 1–4, Sept. 1997.
- [7] G. B. Giannakis and M. K. Tsatsanis, "Signal detection and classification using matched filtering and higher order statistics," *IEEE Trans. Acoustic Speech Signal Processing*, vol. 38, pp. 1284–1296, July 1990.

Moderately Rough Dielectric Interface Profile Reconstruction via Short-Pulse Quasi-Ray Gaussian Beams

Vincenzo Galdi, Julia Pavlovich, W. Clem Karl, David A. Castañon, and Leopold B. Felsen

Abstract—A new technique for estimating the coarse-scale profile of a moderately rough interface between air and a homogeneous dielectric half-space is presented. The proposed approach is based on space-time sparsely sampled reflected field observations and uses a quasi-ray Gaussian beam fast-forward model, coupled with a compact parameterization of the surface profile in terms of B-splines, from which the profile estimation problem is posed as a nonlinear optimization problem. Numerical experiments are presented to assess accuracy, reliability, and computational efficiency. The proposed approach finds applications in adaptive schemes for rough surface underground imaging of shallowly buried targets via ultra wide-band ground penetrating radars.

Index Terms—Gaussian beams (GBs), ground-penetrating radars (GPR), rough surfaces, short pulses.

I. INTRODUCTION

In ground-penetrating radar (GPR) applications, the twice-traversed unknown rough interface separating air and soil acts as a major source of clutter by distorting the interrogating signal on its way to and from the targets of interest, and by generating complicated backscattered field patterns which may obscure the useful signals. Physics-based modeling of such clutter, which could significantly enhance the ultimate GPR performance, poses challenging problems from both the electromagnetic (EM) and signal processing viewpoints. Standard statistical approaches, which tend to model such distortion as additive colored Gaussian noise, perform reasonably well in *detection* problems [1], [2]. However, they have been found to yield limited accuracy and reliability in underground imaging techniques for target *localization* and *classification* (see, e.g., [3]), for which alternative approaches need to be explored. In this connection, we have been investigating a novel *adaptive* framework, based on *quasi-deterministic* compensation of the coarse-scale roughness effect. This approach is based on *prior* estimation of the coarse-scale roughness profile, which is accomplished by utilizing sparse reflected field observation data and fast forward scattering models. In this communication, we address the problem for the case of short-pulse illumination, typical of current ultra wide-band (UWB) GPR systems. The proposed strategy

Manuscript received October 30, 2001; revised February 27, 2002. This work was supported by ODDR&E under MURI Grant ARO DAAG55-97-1-0013 and by the AFOSR under Grant F49620-96-1-0028, and by the Engineering Research Centers Program of the National Science Foundation under Award EEC-9986821. The work of V. Galdi was also supported by a European Union Postdoctoral Fellowship through the University of Sannio, Benevento, Italy. The work of L. B. Felsen was supported in part by the U.S.–Israel Binational Science Foundation, Jerusalem, Israel, under Grant 9900448, and by the Polytechnic University, Brooklyn, NY 11201 USA.

V. Galdi was with the Department of Electrical and Computer Engineering, Boston University, Boston, MA 02215 USA. He is now with the Department of Engineering, University of Sannio, Benevento, Italy (e-mail: vgalidi@unisannio.it).

J. Pavlovich, W. C. Karl, and D. A. Castañon are with the Multidimensional Signal Processing Laboratory, Department of Electrical and Computer Engineering, Boston University, Boston, MA 02215 USA (e-mail: oska@bu.edu; wckarl@bu.edu; dac@bu.edu).

L. B. Felsen is with the Department of Aerospace and Mechanical Engineering and the Department of Electrical and Computer Engineering, Boston University, Boston, MA 02215 USA, and also with the Polytechnic University, Brooklyn, NY 11201 USA (e-mail: lfelsen@bu.edu).

Digital Object Identifier 10.1109/TAP.2003.809857

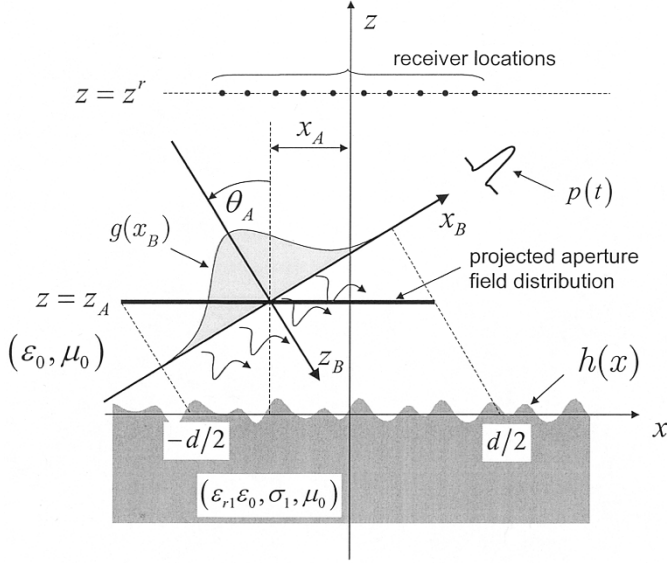


Fig. 1. Problem geometry. An aperture-generated, quasiplane-wave, amplitude-tapered TM-polarized pulsed field impinges from free space onto a dielectric half-space with known relative permittivity ϵ_{r1} and conductivity σ_1 , bounded by a moderately rough interface profile $z = h(\mathbf{x})$. The obliquely incident illumination is projected onto the horizontal aperture plane at $z = z_A$. The reflected field is sampled at N_t time instants at N_r fixed receiver locations $x_1^r, \dots, x_{N_r}^r$ on the observation plane $z = z^r$.

is built on recently developed Gabor-based narrow-waisted *quasi-ray* Gaussian beam (GB) algorithms for short-pulse scattering from moderately rough dielectric interfaces [4]. By exploiting these fast forward models and a low-dimensional spline interface parameterization, together with the (usually small) separation between the rough interface and the target, the prior surface estimation is posed as a nonlinear optimization problem through fitting the model-based prediction to the available *early-time* observation data. The subsequent problem of quasi-deterministic compensation and underground imaging via *late-time* response processing is addressed in a separate paper [5], with particular reference to shallowly buried plastic mine-like targets.

II. STATEMENT OF THE PROBLEM

We consider the two-dimensional (2-D) problem geometry sketched in the (x, z) coordinate space of Fig. 1, where all quantities and fields are assumed to be y -independent. A homogeneous dielectric half-space (soil) of *known* relative permittivity ϵ_{r1} and conductivity σ_1 bounded by a moderately rough interface with profile $z = h(x)$ is illuminated by a y -directed (TM-polarized) pulsed well-collimated EM field, generated by a large truncated aperture field distribution of width d at $z = z_A$. The y -directed incident electric field e^i is assumed to be well approximated by a pulsed truncated amplitude-tapered plane wave

$$e^i(\mathbf{r}, t) \sim g(x_B)p(t - c^{-1}z_B) \quad (1)$$

where $\mathbf{r} \equiv (x, z)$, c is the free-space wavespeed, $p(t)$ is a short pulse of length $T \ll d/c$, and (x_B, z_B) are beam centered coordinates

$$\begin{bmatrix} x_B \\ z_B \end{bmatrix} = \begin{bmatrix} \cos \theta_A & \sin \theta_A \\ \sin \theta_A & -\cos \theta_A \end{bmatrix} \begin{bmatrix} x - x_A \\ z - z_A \end{bmatrix}. \quad (2)$$

In (1) and (2), $g(x_B)$ is a spatial taper, while θ_A and x_A denote the tilt angle of the radiated beam relative to the z axis and its spatial displacement, respectively. Parameters are chosen so that the illumination tapers to zero and vanishes for $|x| > d/2$ (Fig. 1). This synthetic model is

a first step toward understanding the wave physics governing a moderately rough interface, and will provide insights needed when addressing a related class of real-world GPR configurations. At this stage of investigation, we ignore the presence of buried targets, which is dealt with elsewhere [5]. Furthermore, we also neglect the *noisy* (incoherent) contribution of finer-scale roughness, and focus on estimating the coarse scale roughness profile $h(x)$ from sparse reflected field observations.

Estimation of rough surfaces from inverse scattering data has received considerable attention during the past decade. However, most available algorithms (see, e.g., [6]–[9]) have concentrated on conducting surfaces and time-harmonic excitation, and usually require densely sampled measurements. In [10], we addressed this problem for frequency-stepped sparse observations. This approach is extended here to *pulsed* excitation. To proceed, the y -directed reflected electric field is sampled at N_t time instants at N_r fixed receiver locations $x_1^r, \dots, x_{N_r}^r$ at the observation plane $z = z^r$ in Fig. 1; the *known term* in the problem is given by the set of $N_r \times N_t$ samples. In our numerical experiments in Section V, we shall use synthetic field-observation data generated via a full-wave solution of the forward scattering problem (see [4] for details).

III. ROUGH SURFACE FORWARD SCATTERING MODEL

The forward scattering model, detailed in [4], is based on the Kirchhoff Physical Optics (PO) approximation in conjunction with the Gabor-based narrow-waisted pulsed beam (PB) discretization of one-dimensional (1-D) aperture field distributions investigated in [11], and is restricted to moderate roughness (both in height and slope) and slightly lossy soils.

The PO “equivalent current,” which generates the reflected field, is first parameterized in the frequency domain in terms of x domain discretized m -indexed Gabor basis functions with narrow width L , centered on the Gabor lattice points $x_m = mL$; these initial conditions generate narrow-waisted, quasi-ray, complex-source-point GBs propagating along the local reflection directions. For Rayleigh (i.e., differentiated Gaussian) pulses, the resulting time domain analytic Fourier inversion integral can be approximated by rapidly computable closed form expressions, yielding the following approximate PO–PB expansion for the y -directed reflected electric field e^r (see [4] for details)

$$e^r(\mathbf{r}, t) \sim \sum_{|m| \leq (d/2L)} c_m^r b_m^r(\mathbf{r}, t - t_m) \quad (3)$$

where the Gabor expansion coefficients c_m^r and the time delays t_m are determined approximately by sampling the PO equivalent current profile at the lattice points $x_m = mL$, and the PB propagators b_m^r are expressed in terms of rapidly computable confluent hypergeometric functions [4, Sec. IV-B]. The approximate forward scattering model in (3) has been validated and calibrated over various parameter ranges against a rigorous reference solution [4, Sect. V-A], and has been found to provide accurate and robust predictions for moderate roughness (both in height and slope), nongrazing incidence, and slightly lossy soils (see [4, Sec. V-C] for details). Numerical convergence is usually achieved with $d/L \sim 30$ to 100 (narrow-waisted) PBs, resulting in minimal storage requirements and typical computing times of 2 ms per space-time field sample on a 700-MHz PC. Moreover, for computing a number of field time samples at fixed-receiver locations, as required in Section IV, one can take advantage of the structure of the PB propagators in (3) (see [4, Sec. IV-B] for details) to compute the time-independent parts only once, with resulting typical computing times of 20 ms for an *entire* 100-sample waveform, as compared with about 240 s required by our full-wave reference solution. This light computational burden is essential for the overall computational feasibility of the proposed surface estimation approach, with eventual application to subsurface imaging.

IV. SURFACE PROFILE ESTIMATION

Due to the inherent ill-posedness of the surface estimation problem, it is necessary to resort to *regularization* strategies. Acknowledging the implicit limits of retrievable information through inverse scattering, our regularization is based on a compact parameterization of the unknown interface profile function $h(x)$ in a suitable finite-dimensional space. As in [10], we model $h(x)$ using a quartic B-spline parameterization [12] with fixed resolution matched to the coarse level of detail for the reconstruction

$$h(x) = \sum_{n=-4}^{N_h-1} h_n s^{(4)}(x - x_{\min} + n\Delta_x), \quad x_{\min} \leq x \leq x_{\max} \quad (4)$$

whereby the coefficients h_n become the *unknowns* of the problem. In (4), $s^{(4)}(\cdot)$ is a standard quartic B-spline basis function [12] (see also [10, eq. (5)]) with finite spatial support $5\Delta_x$, where $\Delta_x = (x_{\max} - x_{\min})/N_h$ denotes a scale parameter whose choice can be guided by possible prior information and refined *adaptively* (see Section V). To prevent ill-conditioning, it is crucial that the number of unknown parameters to be retrieved does not substantially exceed the *essential* dimension of the observation data set. For the problem of interest here, involving UWB pulsed excitation and *close proximity* setup, quantifying the essential information contained in the observed field as well as the effect of utilized prior information, is not straightforward. However, the number of unknowns in the inverse problem is strongly related to the type of roughness, the adopted parameterization, the extent of the reconstruction interval, and the finer scales one is willing to neglect. In this preliminary investigation, we did *not* attempt to address *optimal* strategies for profile parameterization and data acquisition. Instead, we pursued a more *pragmatic* approach. Under our stated problem conditions, we obtained reasonably accurate and robust reconstructions, with a reasonably small number of unknowns ($N_h \lesssim 30$), via an adaptive strategy (see Section V). Using our PO-PB fast forward model in [4] in conjunction with the spline interface profile parameterization in (4), the well-posedness of the problem is restored by estimating the unknown parameters via *fitting* the model-based forward scattering prediction to the available observation data, i.e., minimizing a suitable *cost functional*. We use a simple least square formulation

$$J(\underline{h}) = \|\underline{\hat{e}}^r(\underline{h}) - \underline{\hat{e}}^r\|^2 = \sum_{p=1}^{N_r} \sum_{q=1}^{N_t} \gamma_p (e_{pq}^r - \hat{e}_{pq}^r)^2 \quad (5)$$

where $\hat{e}_{pq}^r \equiv \hat{e}^r(\mathbf{r}_p^r, t_{pq})$ denotes the y -directed reflected field *observed* at time $t_{pq} \in [T_p^{(on)}, T_p^{(off)}]$ at receiver locations $\mathbf{r}_p^r = (x_p^r, z^r)$ (Fig. 1), $e_{pq}^r \equiv e^r(\mathbf{r}_p^r, t_{pq}; \underline{h})$ denotes the corresponding *forward prediction* for the surface profile coefficients $\underline{h} = \{h_{-4}, \dots, h_{N_h-1}\}$, and γ_p are normalization coefficients. Anticipating the possible presence of buried targets, dealt with in [5], the observation intervals $[T_p^{(on)}, T_p^{(off)}]$ are chosen so as to gate out the *late-time* response (i.e., causal contributions from regions beyond a critical depth), in order to prevent any possible bias in the surface profile estimation.

In general, the predictive forward model $e^r(\mathbf{r}_p^r, t_{pq}; \underline{h})$ is a nonlinear function of the coefficients \underline{h} . Therefore, the cost functional in (5) is generally *nonconvex* with respect to \underline{h} and may have multiple local minima which correspond to *false solutions*. Standard descent-based optimization techniques (e.g., conjugate gradient [13]) can lead to falsely trapped solutions unless an accurate initial guess is available. For the frequency-stepped configuration in [10], the smoothness of the cost functional was found to be essentially dependent on the frequency

content of the excitation field, and a multiresolution *frequency-hopping* strategy [14] was devised to achieve the global optimization (see [10, Sec. III-C] for details). The same guidelines can be applied to the pulsed excitation of interest here, with the pulse length cT now playing the key role. In particular, *short* pulses are desirable to enhance resolution and accuracy in the reconstruction, but an exceedingly wide-band excitation would most likely yield a highly nonconvex cost functional with many local minima, whose global minimization could become computationally unfeasible. In our numerical investigation, we found that values of $cT \lesssim 0.2d$ tend to produce undesired local minima in the cost functional, whereas for $cT \gtrsim 0.5d$, the achieved resolution deteriorates (see Fig. 3). Moreover, for the eventual underground imaging problem of interest (see [5]), it is also essential to achieve adequate soil penetration, and therefore operate at sufficiently low frequencies. In principle, one could gain more flexibility by using different sets of pulses for the surface estimation (e.g., implementing multiresolution optimization strategies as in [10]) and for the underground imaging, at the expense of hardware complexity. However, in our numerical experiments, we found that a *single* pulse in the typical UWB GPR frequency range (e.g., as in Fig. 2(a) with $cT \sim 0.4d$, i.e., $T \sim 1.3$ ns for $d = 1$ m) can be used for *both* surface estimation *and* underground imaging of shallowly buried targets (see [5]), thus having the potential of yielding a reasonable tradeoff between the above contrasting requirements.

V. NUMERICAL RESULTS

As mentioned earlier, the needed reflected field-observation data in (5) were simulated via a reliable full-wave reference solution of the forward scattering problem, based on the time-harmonic multifilament current method in [15] and the fast Fourier transform (see [4, Sec. V-A] for details). Forward predictions in (5) were generated via the PO-PB model in (3) with $d/L = 40$ beams, for which the accuracy was preliminarily verified.

We begin with a simplified configuration where we use as a template for inversion *the same* spline model that was used for *generating* the *actual* profile. In other words, we assume *a priori* knowledge of the scale parameter Δ_x in (4) (i.e., the number of B-spline basis functions), and focus on retrieving the unknown coefficients h_n only. This somewhat unrealistic assumption will be removed subsequently via an iterative *adaptive* framework. In all simulations below, a *cosine-tapered normally-incident* excitation was used with $g(x) = \cos(\pi x/d)$, $\theta_A = x_A = 0$, and a single fourth-order Rayleigh pulse with $cT = 0.4d$ [Fig. 2(a)], which was found by trial and error to provide a good compromise between resolution and smoothness of the cost functional. An observation time window $[T_p^{(on)}, T_p^{(off)}]$ with $cT_p^{(on)} = 0.3d$ and $T_p^{(off)} = 0.8d$, $p = 1, \dots, N_r$, was used, so as to roughly gate out scattering contributions from possible targets buried deeper than ~ 8 cm below nominal ground ($z = 0$). The resulting cost functional in (5) was minimized via the Polak-Ribiere version of the conjugate gradient (CG) algorithm (particularly suited for nonquadratic functions [13]). The needed gradient of J was computed using a central difference formula, resulting in $2N_h + 8$ functional evaluations (i.e., $2N_h + 8$ solutions of a forward scattering problem), $N_h + 4$ being the number of unknown spline coefficients in (4). Loose *a priori* knowledge was exploited by using as an initial guess a flat interface at $z = 0$ (i.e., $\underline{h} = \underline{0}$) and restricting the surface profile search to ± 8 cm around it.

A typical reconstruction example is shown in Fig. 2(b). The surface profile realization was generated using the quartic-spline model in (4) with random coefficients. Although no specific roughness model (e.g., Gaussian) was simulated, geometric and constitutive parameters were selected so as to mimic natural moderate roughness with maximum-to-minimum height ~ 4 cm and maximum slope $\sim 32^\circ$ for a class of realistic soils [16]. The reconstruction is reasonably accurate

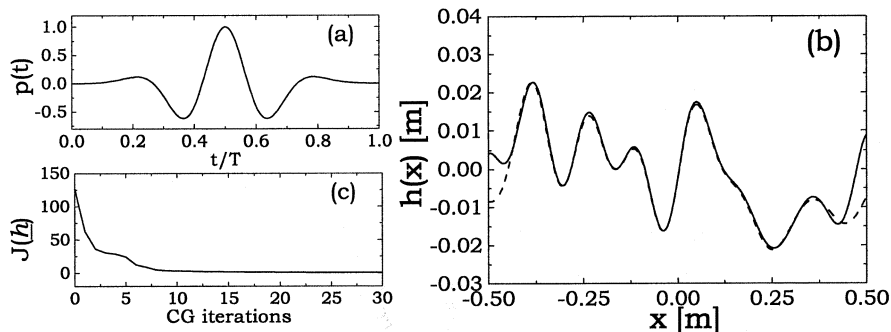


Fig. 2. Rough surface profile reconstruction. Geometry as in Fig. 1, with $g(x) = \cos(\pi x/d)$, $d = 1$ m, $\theta_A = 0$, $x_A = 0$, $z_A = 0.1$ m. The rough surface profile realization was randomly generated via the spline model in (4) with $x_{\min} = -0.55$ m, $x_{\max} = 0.55$ m, $N_h = 16$, so as to simulate typical moderate roughness (maximum height ~ 4 cm maximum-to-minimum, maximum slope $\sim 32^\circ$) for a class of realistic soils ($\epsilon_{r1} = 4$, $\sigma_1 = 0.01$ S/m). For the surface profile estimation, the reflected field is sampled at $N_r = 11$ receivers and $N_t = 50$ time instants at $z^r = 0.3$ m and $x_p^r = -0.5$ m, -0.4 m, \dots , 0.5 m, with $cT_p^{(on)} = 0.3d$ and $cT_p^{(off)} = 0.8d$, $p = 1, \dots, N_r$. Normalization coefficients in (5): $\gamma_p = 1$, $p = 1, \dots, N_r$. (a): Fourth-order Rayleigh pulsed excitation $p(t)$ ($cT = 0.4d$, i.e., $T \sim 1.3$ ns). (b) — Actual profile; - - - Reconstruction. (c) Corresponding cost functional in (5) versus number of CG iterations.

throughout most of the interval, except near the edges of the illuminated region. The likely explanation for this loss of accuracy, also observed in [10], is due to the weak illumination in these regions, which is attributed to the aperture field (cosine) tapering but was required to avoid numerical artifacts (edge effects). This order of accuracy was observed in many numerical experiments, with numerical convergence of the minimization algorithm typically achieved within ~ 30 CG iterations [see Fig. 2(c)], resulting in computing times of ~ 55 secs on a 700 MHz PC. No particular effort was made to fully optimize the numerical implementation. In this connection, significant speed-up can be expected through the use of more effective (e.g., analytic) approaches to compute the gradient of the cost functional.

The influence of the pulse length cT in the smoothness of the cost functional in (5) is illustrated in Fig. 3, which shows representative cuts of the cost functional for values of $cT/d = 0.15$, 0.4 , and 0.55 . The cut direction in the \underline{h} space is specified by

$$\underline{h}_c = (1 - \alpha)\underline{h}_a, \quad -1 \leq \alpha \leq 2 \quad (6)$$

where \underline{h}_a indicates the *actual* value of the spline coefficient array, and α parameterizes the spanning, with $\alpha = 0$ and $\alpha = 1$ corresponding to the actual interface and to the initial guess (flat interface at $z = 0$, i.e., $\underline{h} = 0$), respectively. It is observed from Fig. 3 that in all cases, the cost functional exhibits a deep *global* minimum at $\alpha \approx 0$. For the shortest pulse ($cT = 0.15d$), however, it also has some *local* minima and saddle points. As the pulse length is increased ($cT = 0.4d, 0.55d$), the local minima and saddle points are gradually wiped out, and the basin of attraction of the global minimum becomes larger and larger, thus facilitating the global optimization via standard descent-based techniques. Exceedingly long pulses (e.g., $cT = 0.55d$), however, tend to produce rather flat global minima, with a consequent loss of resolution, and a possible bias in the position of the minimum due to inaccuracy in this case of the (short-pulse asymptotic) PO–PB forward model. As already mentioned in Section IV, the best reconstruction results were obtained for values of $cT \sim 0.4d$ (as in Fig. 2); values of $cT \lesssim 0.2d$ were found susceptible to yielding *false solutions*, whereas values of $cT \gtrsim 0.5d$ were found to yield *poorer resolution*.

Concerning the choice of data size and receiver locations, the parameters used are consistent with those typically encountered in realistic UWB GPR systems. The algorithm was calibrated for observation heights z^r ranging from 20 to 50 cm, number of receivers ranging from 5 to 20 (i.e., receiver spacing ranging from $1.6 \lambda_c$ to $0.4 \lambda_c$, with λ_c denoting the free-space wavelength at the center frequency of the pulse), and number of samples N_t ranging from 20 to 200. The parameters

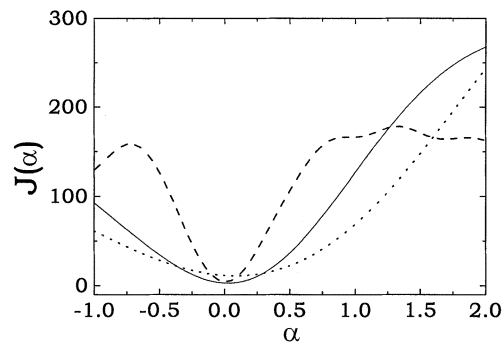


Fig. 3. Parameters as in Fig. 2. Representative cuts of the cost functional in (5), along the direction in (6), for various values of cT . — $cT = 0.4d$; - - - $cT = 0.15d$; $cT = 0.55d$.

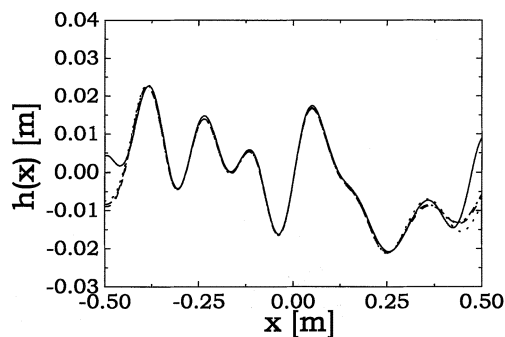


Fig. 4. Parameters as in Fig. 2. Surface profile reconstruction examples with uncertain or corrupted data. — Actual profile; - - - Reconstruction with +10% error in ϵ_{r1}, σ_1 ; Reconstruction with -10% error in ϵ_{r1}, σ_1 ; - · - · - Reconstruction with observation data corrupted by $\pm 10\%$ uniform noise.

used in Fig. 2, arrived at through trial and error compromising between accuracy and computational burden, were found to yield (average) resolution on the order of 2 to 3 mm. Concerning the choice of the normalization coefficients γ_p in the cost functional (5), the best reconstruction results (as in Fig. 2) were found for $\gamma_p = 1$, $p = 1, \dots, N_r$. The likely explanation is that this choice helps de-emphasizing the effect of the edge receivers, for which the scattered field predictions from our PO–PB forward model are somewhat less accurate.

In order to assess the reliability of the surface profile estimation algorithm, we performed a number of sensitivity tests with respect to possible uncertainty in the prior knowledge, as well as corruption in the observed data. Fig. 4 displays typical reconstructions obtained by

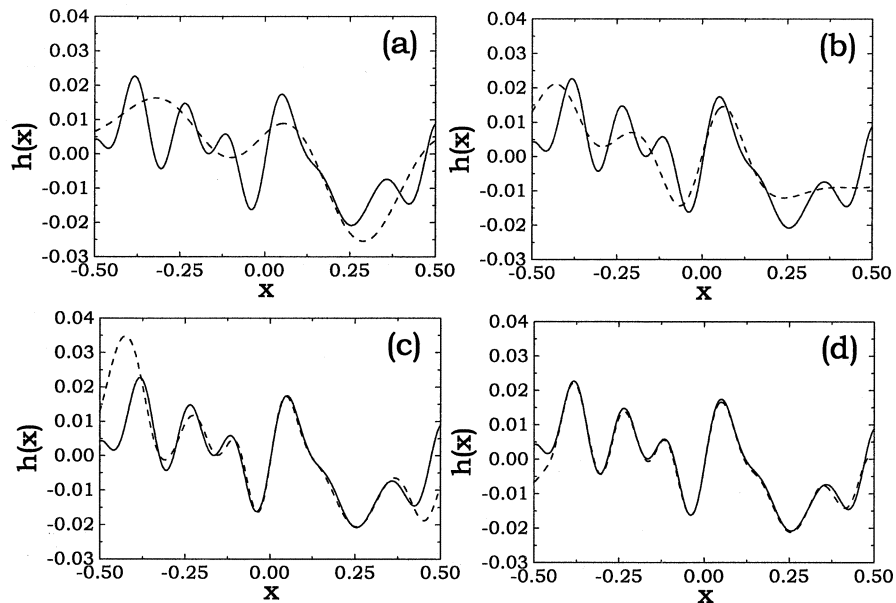


Fig. 5. Parameters as in Fig. 2. Example of iterative adaptive spline parameterization. (a): Reconstruction using a tentative initial coarse parameterization ($N_h = 6$) and a flat interface initial guess (number of CG iterations: $N_{CG} = 8$; final value of cost functional: $J^{(\min)} = 70.4$); (b), (c), (d): Refinements obtained by progressively increasing the number of basis functions, $N_h = 12, 18, 24$, respectively, and using the previous stage reconstruction as initial guess ($N_{CG} = 12, 12, 23$, respectively; $J^{(\min)} = 26, 3.7, 0.53$, respectively). — Actual profile; - - - Reconstruction.

introducing a $\pm 10\%$ error in the values of the soil parameters ϵ_{r1} and σ_1 used in the forward scattering model, and by using observation data corrupted by $\pm 10\%$ uniform noise. As one can see, the surface estimation algorithm turns out to be remarkably robust.

Finally, to remove the unrealistic perfectly-matched-template assumption, we now invoke an adaptive iterative framework for estimating the surface profile in Fig. 2(b), which was generated via the B-spline model in (4) with $N_h = 16$, by postulating a *mismatched* spline template (i.e., $N_h \neq 16$). Referring to Fig. 5, the procedure is started with a tentative initial coarse parameterization ($N_h = 6$) and the usual flat-interface ($z = 0$) initial guess for the profile, which leads to the corresponding gross-scale reconstruction in Fig. 5(a). The resolution is gradually increased, utilizing at each stage the previous stage reconstruction as the initial guess. Fig. 5(b)–(d), for instance, show the iterative improvements obtained via the sequence $N_h = 12, 18, 24$ (deliberately chosen so as to avoid the perfectly matched case $N_h = 16$), with the spline parameterization progressively tuned so as to capture the various details in the surface profile. The accuracy in the last stage reconstruction [Fig. 5(d)] is comparable to that achieved with a perfectly-matched template [Fig. 2(b)]. In this example, a pragmatic stopping criterion was used based on the (in) sensitivity of the cost functional with respect to further increases in N_h . Specifically, a maximum of 30-CG iterations was used in each reconstruction stage, and N_h was increased until the decreasing rate in the cost functional between two subsequent iterations was found to be less than 1%. Although no attempt was made to find an optimal updating schedule for N_h , a satisfactory tradeoff between reconstruction quality and computational burden was found for $\sim 20\%$ N_h increase. More systematic approaches based, e.g., on the *minimum description length* principle, can be found in [17]. Also, more flexible *multiscale* parameterizations can be applied in principle to deal with more complex surface profiles, but this is outside the scope of the present paper.

VI. CONCLUSION

In this communication, we have presented a novel inversion algorithm for the reconstruction of moderately rough dielectric interfaces, using space–time sparsely sampled reflected field data. The proposed

algorithm has been found to provide fast, accurate, and robust estimations for moderate roughness (~ 4 cm maximum-to-minimum, maximum slopes $\lesssim 40^\circ$), even for noisy data and with imperfect knowledge of soil parameters. These results lay the foundation for the adaptive techniques for subsurface GPR image reconstruction of shallowly buried plastic mine-like targets in the presence of rough air–soil interfaces addressed in [5]. Extensions presently under investigation include generalization to fully three-dimensional geometries.

REFERENCES

- [1] T. Dogaru, L. Collins, and L. Carin, "Optimal time-domain detection of a deterministic target buried under a randomly rough interface," *IEEE Trans. Antennas Propagat.*, vol. 49, pp. 313–326, Mar. 2001.
- [2] H. Zhan, C. M. Rappaport, M. El-Shenawee, and E. L. Miller, "Mine detection under rough ground surfaces using 2-D FDTD modeling and hypothesis testing," in *Proc. 2001 IEEE Antennas Propagat. Int. Symp.*, vol. 3, Boston, MA, July 8–13, 2001, p. 756.
- [3] H. Feng, D. A. Castañón, W. C. Karl, and E. L. Miller, "GPR imaging approaches for buried plastic landmine detection," in *Detection and Remediation Technologies for Mines and Minelike Targets V*, A. C. Dubey, J. F. Harvey, J. T. Broach, and E. R. Dugan, Eds. Orlando, FL: Int. Society Opt. Eng., Aug. 2000, vol. 4038, pp. 1485–1496.
- [4] V. Galdi, L. B. Felsen, and D. A. Castañón, "Quasiray Gaussian beam algorithm for short-pulse two-dimensional scattering by moderately rough dielectric interfaces," *IEEE Trans. Antennas Propagat.*, vol. 51, pp. 171–183, Feb. 2003.
- [5] V. Galdi, H. Feng, D. A. Castañón, W. C. Karl, and L. B. Felsen, "Moderately rough surface underground imaging via short-pulse quasiray Gaussian beams," *IEEE Trans. Antennas Propagat.*, vol. 51, Sept. 2003, to be published.
- [6] R. J. Wombell and J. A. DeSanto, "Reconstruction of rough-surface profiles with the Kirchhoff approximation," *J. Opt. Soc. Amer. A*, vol. 8, no. 12, pp. 1892–1897, Dec. 1991.
- [7] A. Schatzberg and A. J. Devaney, "Rough surface inverse scattering with the Rytov approximation," *J. Opt. Soc. Amer. A*, vol. 10, no. 5, pp. 942–950, May 1993.
- [8] C. Ying and A. Noguchi, "Rough surface inverse scattering problem with Gaussian beam illumination," *IEICE Trans. Electron.*, vol. E77-C, no. 11, pp. 1781–1785, Nov. 1994.
- [9] K. Harada and A. Noguchi, "Reconstruction of two dimensional rough surface with Gaussian beam illumination," *IEICE Trans. Electron.*, vol. E79-C, no. 10, pp. 1345–1349, Oct. 1996.

- [10] V. Galdi, D. A. Castañón, and L. B. Felsen, "Multifrequency reconstruction of moderately rough interfaces via quasiray Gaussian beams," *IEEE Trans. Geosci. Remote Sensing*, vol. 40, pp. 453–460, Feb. 2002.
- [11] V. Galdi, L. B. Felsen, and D. A. Castañón, "Narrow-waisted Gaussian beam discretization for short-pulse radiation from one-dimensional large apertures," *IEEE Trans. Antennas Propagat.*, vol. 49, pp. 1322–1332, Sept. 2001.
- [12] L. L. Shumaker, *Spline Functions: Basic Theory*. New York: Wiley, 1981.
- [13] W. H. Press, S. A. Teukolsky, W. T. Vetterling, and B. P. Flannery, *Numerical Recipes in C: The Art of Scientific Computing*, 2nd ed. Cambridge, UK: Cambridge Univ. Press, 1992.
- [14] W. C. Chew and J. H. Lin, "A frequency-hopping approach for microwave imaging of large inhomogeneous bodies," *IEEE Microwave Guided Wave Lett.*, vol. 5, pp. 439–441, Dec. 1995.
- [15] Y. Leviatan and A. Boag, "Analysis of electromagnetic scattering from dielectric cylinders using a multifilament current model," *IEEE Trans. Antennas Propagat.*, vol. 35, pp. 1119–1127, Oct. 1987.
- [16] J. E. Hipp, "Soil electromagnetic parameters as functions of frequency, soil density, and soil moisture," *Proc. IEEE*, vol. 62, p. 9103, Jan. 1974.
- [17] J. Rissanen, *Stochastic Complexity in Statistical Inquiry*, ser. Series in Computer Science. Singapore: World Scientific, 1989, vol. 15.